Colloids and Surfaces A 602 (2020) 125106

Contents lists available at ScienceDirect

Colloids and Surfaces A

journal homepage: www.elsevier.com/locate/colsurfa

Preparation of wide-angle and abrasion-resistant multi-layer antireflective coatings by MgF_2 and SiO_2 mixed sol

Xiaoyu Sun[a,b], Jielei Tu[a,b,*], Lei Li[a,b], Weinan Zhang[a,b], Kai Hu[a,b]

[a] Yunnan Normal University, School of Energy and Environment Science, Kunming, 650500, China
[b] Yunnan Key Laboratory of Rural Energy Engineering in Yunnan Province, Kunming, 650500, China

GRAPHICAL ABSTRACT

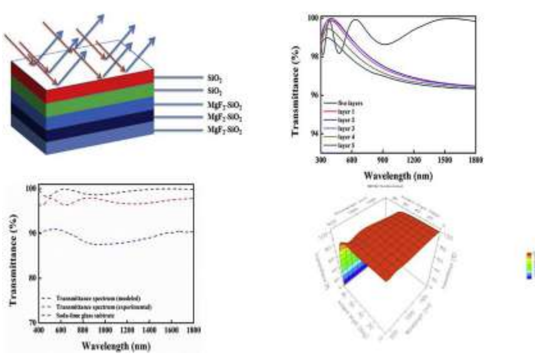

ARTICLE INFO

Keywords:
Antireflective coating
SiO_2
Wide-angle
MgF_2
Broadband
Sol–gel

ABSTRACT

The wide-angle broadband antireflective coatings (ARCs) were fabricated by a sol–gel method and covered on a soda-lime glass substrate by using dip-coating process. The crystal structural, morphological and antireflection performance of ARCs were characterized by X-ray diffraction (XRD), field emission scanning electron microscopy (FESEM), ultraviolet spectrophotometer (UV–vis), etc. In addition, the optimal experimental parameters of each coating were obtained by optical film design software combined with experimental characterization. The average transmittance of the wide-angle broadband ARCs is 9% higher than 88.90 % of the soda-lime glass substrate in the range of 400 − 1200 nm. Furthermore, the preliminary evaluation of wear resistance shows that the antireflective performance of the coating was stable before and after the friction test. All the excellent antireflective performance and abrasion-resistance afforded the ARCs with potential application in fields of construction, medical, new energy, military, etc.

1. Introduction

Antireflective coatings (ARCs) can effectively reduce unwanted reflection losses and improve the needful transmittance in an extensive wavelength range and has been widely used in many related equipment such as construction glass, computer display screen, military equipment, light-emitting diodes, architectural glasses, windscreens and high power laser system [1–3]. Especially in the photovoltaic field, the antireflection film glass used in solar photovoltaic can significantly enhance the photoelectric conversion efficiency of solar cells, reduce the cost of photovoltaic power generation, and enhance their comprehensive competitiveness in the market. To fabricate ARC, different

* Corresponding author.
E-mail address: tjl@ynnu.edu.cn (J. Tu).

https://doi.org/10.1016/j.colsurfa.2020.125106
Received 9 April 2020; Received in revised form 22 May 2020; Accepted 30 May 2020
Available online 01 June 2020
0927-7757/

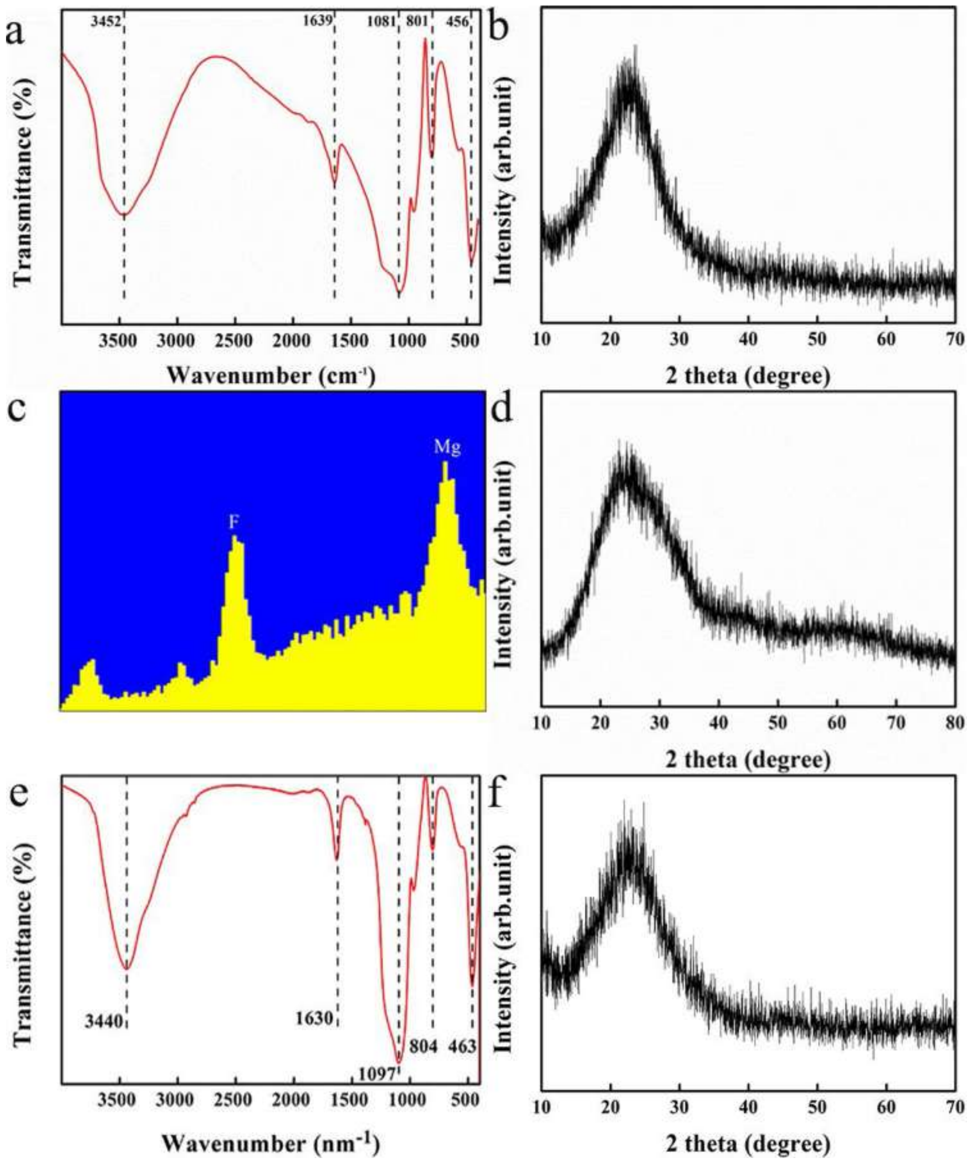

Fig. 1. The FT-IR spectra of (a) base-catalyzed SiO_2 and (e) acid-catalyzed SiO_2 sol. The XRD curves of (b) base-catalyzed SiO_2, (d) MgF_2 and (f) acid-catalyzed SiO_2 coating. The EDX image of (c) MgF_2..

method have been used, including reactive ion etching [4], electron beam (e-beam) evaporation, magnetron sputtering, plasma-enhanced chemical vapor deposition (PECVD) [5,6], Atomic layer deposition (ALD) [7] and sol-gel process together either with layer-by-layer [8], spin-coating [9,10], dip-coating [11] or spray-coating process [12]. Among these preparation methods, the sol-gel process has been used to obtain various antireflective thin films in view of its simple craft, low cost, high quality and mass production [13,14]. Thus, the sol-gel method has become the mainstream method for preparing ARC on the glass surface of photovoltaic module cover plates. In the past few years, all kind of materials with potential applications are used to make anti-reflection coatings, such as: TiO_2, SiC–SiO_2, Al_2O_3, SiO, ZnO, CaF_2, ZnSe, SiO_2-TiO_2, ZnS, a-SiNx, Ta_2O_5 and Si_3N_4 [15–25]. According to Fresnel theory, the reflectance of solar photovoltaic glass can be given by:

$$R = \left(\frac{n_{air}n_s - n_1^2}{n_{air}n_s + n_1^2}\right)^2 \tag{1}$$

where R, n_s, n_{air} and n_1 are the reflectance, the refractive index of the substrate, incident medium and coating, respectively [26,27]. From Eq. (1), it can be seen that when n_0 and n_1 are equal, the reflectance can reach 0%. Beside, covering the surface of the exit medium with an antireflection coating is an effective measure to meet the above conditions. To obtain the minimum reflectance, the optimal refractive index can be calculated follow:

$$n_1 = (n_{air}n_s)^{1/2} \tag{2}$$

where n_1, n_{air} and n_s are refractive indexes of the ARCs, incident medium (air, $n1 = 1$) and substrate (soda-lime glass, $ns = 1.51$), respectively [28]. Therefore, if the surface of a soda-lime glass covered with ARC needs to obtain 100 % transmittance, the optimal refractive index of ARC should be 1.22. Agustín-Sáenz et al. prepared a multi-functional ARC applied to the field of concentrated solar energy by sol-gel process and explored the influence of sintering temperature on the durability of the coating [29]. Chen et al. have been prepared a ZnO nanorod array as ARCs by using a sol-gel method. The ZnO ARC can improve the efficiency of polycrystalline silicon solar energy from 10.4%–12.8% through a light-capturing structure [30].

However, the antireflection performances of these coatings were limited by its structure, that is, refractive index or number of layers of the coating. In addition, ARCs must ensure stable and high

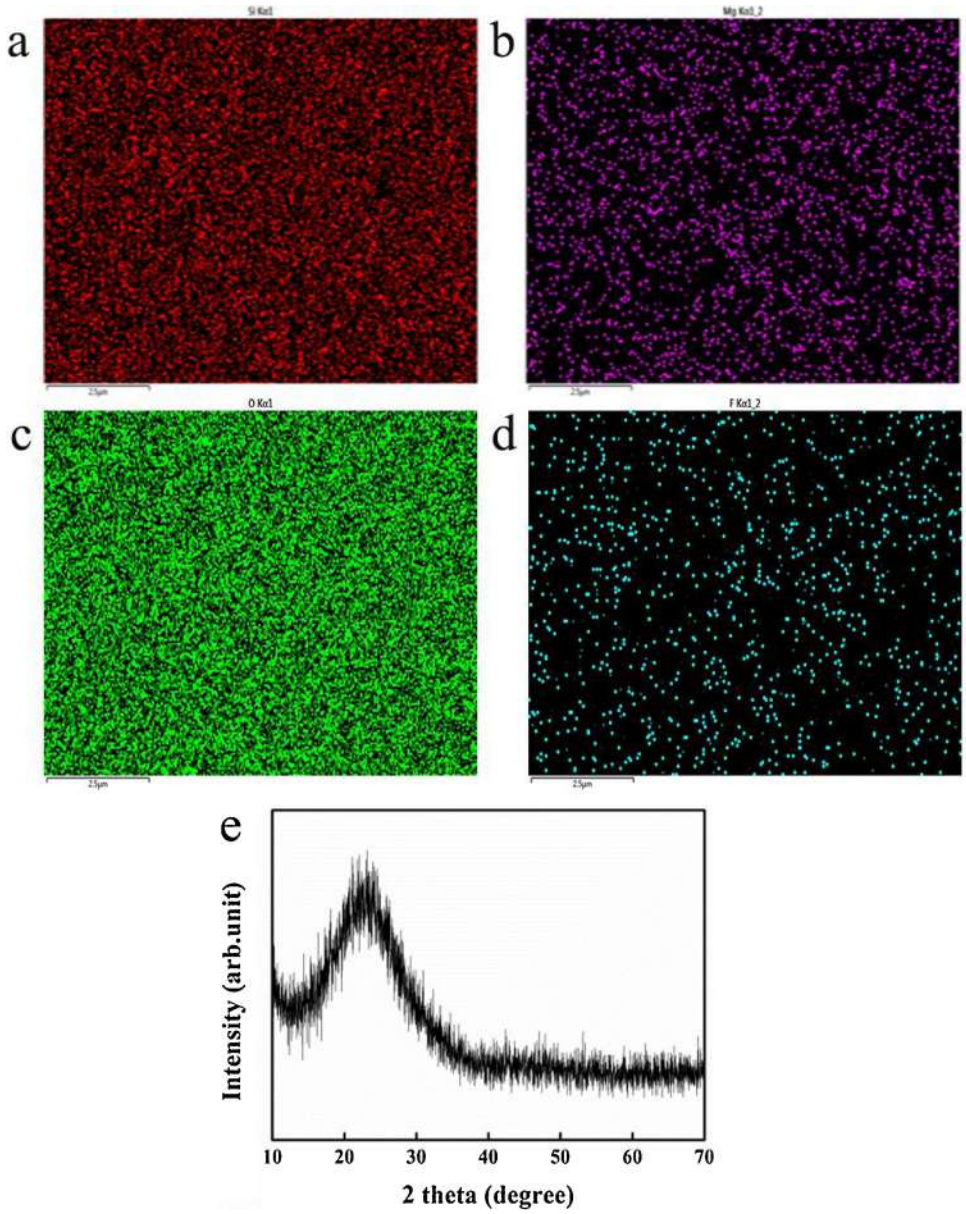

Fig. 2. Scanning electron microscope images of the EDX mapping (a)-(d) and the XRD image of (e).

Table 1
The parameters of each coating that makes up the wide-angle broadband ARC are obtained by Macleod.

Layer position	material	thickness (nm)	The refractive index (λ = 550 nm)
Layer 1	SiO_2	78.85	1.12
Layer 2	SiO_2	79.95	1.15
Layer 3	MgF_2-SiO_2	80.09	1.20
Layer 4	MgF_2-SiO_2	79.96	1.25
Layer 5	MgF_2-SiO_2	80.00	1.28

transmittance during long-term use. To achieve this goal, ARCs must have some characteristics such as abrasion resistance, photocatalysis and superhydrophobic [31–40]. Tao et al. used a sol-gel dip coating process to prepare a multifunctional ARC composed of base-catalyzed SiO_2 nanoparticle, hollow SiO_2 nanoparticle and TiO_2 nanoparticle. This coating has been proven to be stable under severe conditions of high temperature and high humidity through multiple evaluation tests optical performance [41]. Jannat et al. developed a sol-gel spin coating process to prepare SiC–SiO_2 ARC for crystalline silicon solar cells [42].

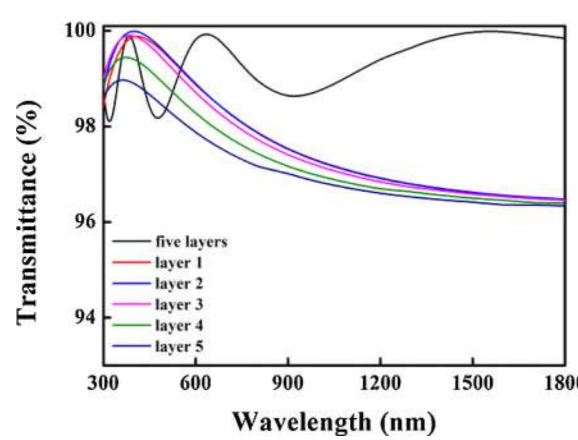

Fig. 3. The transmittance curves of the substrates coated with layer 1, layer 2, layer 3, layer 4, layer 5 and wide-angle broadband ARC at the incident angle of 0°, respectively.

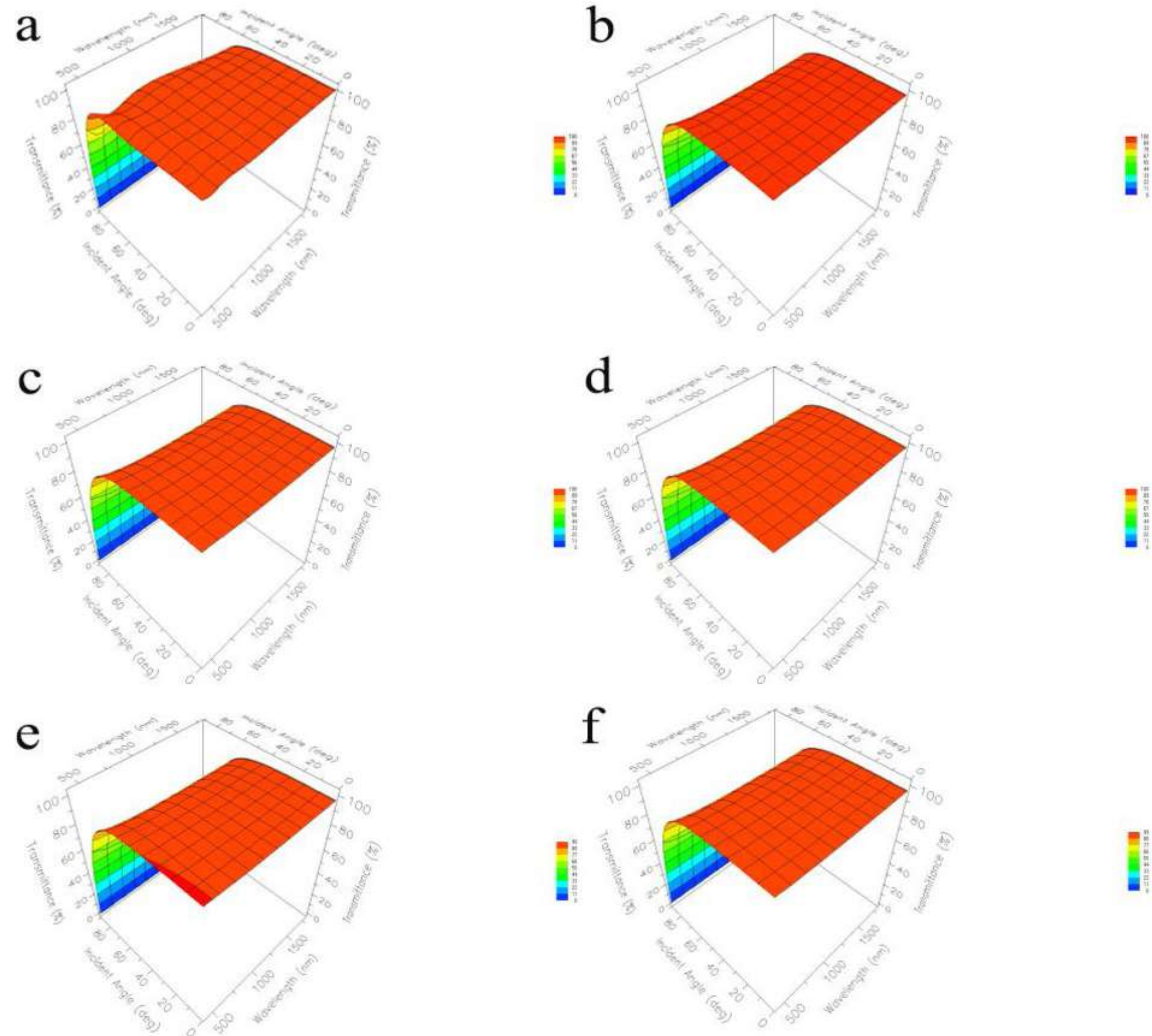

Fig. 4. The three-dimensional graph of transmittance with single (b) layer 1, (c) layer 2, (d) layer 3, (e) layer 4, (f) layer 5 and (a) wide-angle broadband ARC at different incident angles (0-90°) and wavelengths (300-1800 nm).

Lien et al. successfully prepared TiO_2 monolayer, SiO_2/TiO_2 bilayer and SiO_2/SiO_2-TiO_2/TiO_2 multilayer ARCs on the monocrystalline Si solar cells by spin-coating process [43]. However, these layers are only single-layer or double-layer structures and cannot achieve broadband antireflection performance.

In this research, wide-angle broadband ARC was prepared by sol-gel method. We fabricated low refractive index SiO_2 coatings and MgF_2-SiO_2 composite coatings with different refractive index using the dip-coating process. Multilayer wide-angle broadband ARCs can be obtained by using SiO_2 with MgF_2-SiO_2 coatings with different refractive indices. The optimal parameters of each coating that make up the multilayer film were obtained through a combination of film design software and experiments. Meanwhile, the effect of various factors on the property of the coating during the preparation process was investigated. Besides, the abrasion resistance of the multilayer wide-angle broadband ARCs was measured initially by friction test. The soda-lime glass coated with wide-angle broadband ARCs has a significantly higher transmittance than the pure substrate in a wide wavelength range of $400-1200$ nm. Compared with electron beam evaporation, magnetron sputtering and atomic layer deposition technology, these processes have the advantages of low cost, simple operation, and are suitable for large-scale commercial production. The ARCs may have huge market potential in areas such as new energy power generation.

2. Experimental details

2.1. Materials

Soda-lime glass (South China Xiangcheng Technology, Changsha, China) of $20 \times 70 \times 1.5mm$ were used as the substrates. Absolute ethanol (EtOH, 99 %) and Methanol (MeOH, 99 %) were obtained from Tianjin. Tetraethoxysilane (TEOS, 99 %), nitric acid (HNO_3, 97 %), hydrofluoric acid (HF, 40 %) and ammonia ($NH_3{\cdot}H_2O$, 28 %) were all obtained from Tianjin Fengchuan Chemical Reagent Technology Co., Ltd. Magnesium acetate tetrahydrate ($Mg(Ac)_2{\cdot}4H_2O$, 99 %) was obtained from Aladdin. Triton X-100 (TX-100, 98 %) was purchased from Macklin. All reagents and solvents were of analytical reagent grade. The water (H_2O) was deionized by distilled water manufacturing system. The acid-catalyzed SiO_2, base-catalyzed SiO_2 and MgF_2 sol used in the preparation process are all self-made in the laboratory.

2.2. Preparation of SiO_2 sol

The acid-catalyzed SiO_2 sol was prepared according to Hao et al.

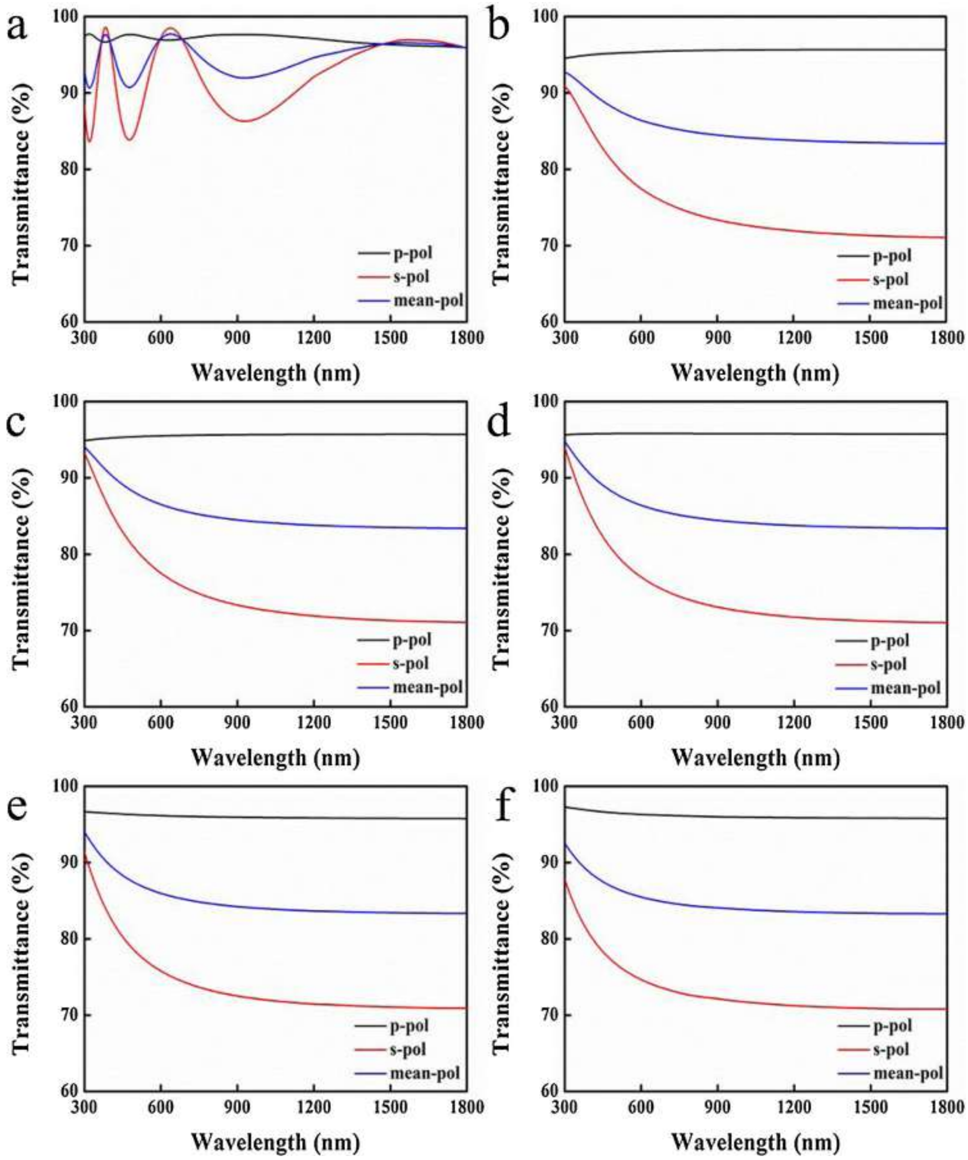

Fig. 5. The transmittance curves with single (b) layer 1, (c) layer 2, (d) layer 3, (e) layer 4, (f) layer 5 and (a) wide-angle broadband ARC at incident angle of 70°, where p-pol, s-pol and mean-pol represent p-polarized, s-polarized and average transmittances, respectively.

Table 2
Influence of temperature on the performance parameters of MgF_2 coatings.

Samples	temperature/°C	time/h	n	d/nm	porosity/%
M-100	100	24	1.35	79.6	80
M-130	130	24	1.28	81.4	82
M-160	160	24	1.19	83.1	87
M-190	190	24	1.17	85.9	89
M-210	210	24	1.15	85.6	92

report [44]. The acid-catalyzed SiO_2 sol was synthesized using TEOS as precursor, HNO_3 as catalyst and EtOH as solvent. Then, TEOS, EtOH, H_2O, and HNO_3 in a molar ratio of 1: 10: 15: 0.05 were mixed under stirring for 2 h and aged for 24 h. The base-catalyzed SiO_2 sol was prepared based on the procedure used by Stöber et al. [45]. TEOS, EtOH, $NH_3{\cdot}H_2O$ and H_2O with molar ratio of 1:180:3:16 were mixed and stirred for 2 h at room temperature, then aged for 3 days to get sol.

2.3. Preparation of SiO_2 sol with low refractive index

The base-catalyzed SiO_2 sol was obtained based on the process used by Section 2.2 above. After being aged for 24 h, the TX-100/SiO_2 mixed sol with TX-100 concentration of 0, 5, 10, 15, 18, 20, 25, 30, 35, 40 45 and 50 g/L was obtained By adding TX-100 with different volume fractions into the solution. The sols are denoted as "A-X", in which X means the TX-100 concentration. That is, the sols prepared from various TX-100 concentrations (from 0 to 50) are abbreviated as A-0, A-5, A-10, A-15, A-18, A-20, A-25, A-30, A-35, A-40, A-45, and A-50, respectively.

2.4. Preparation of MgF_2 sol

The MgF_2 sol was synthesized by hydrolysis and polymerization reactions of in $Mg(OAc)_2$ the catalyst of HF. 1.96 g of $Mg(OAc)_2$ and 80 mL of MeOH were first mixed until the solution was homogenous. Then, 0.3 mL of HF was tardily added into a MeOH solution of Mg $(OAc)_2$ under vigorous stirring. Finally, the mixed solution was reacted at 100, 130, 160, 190 and 210 °C for 24 h. The sols are denoted as "M-

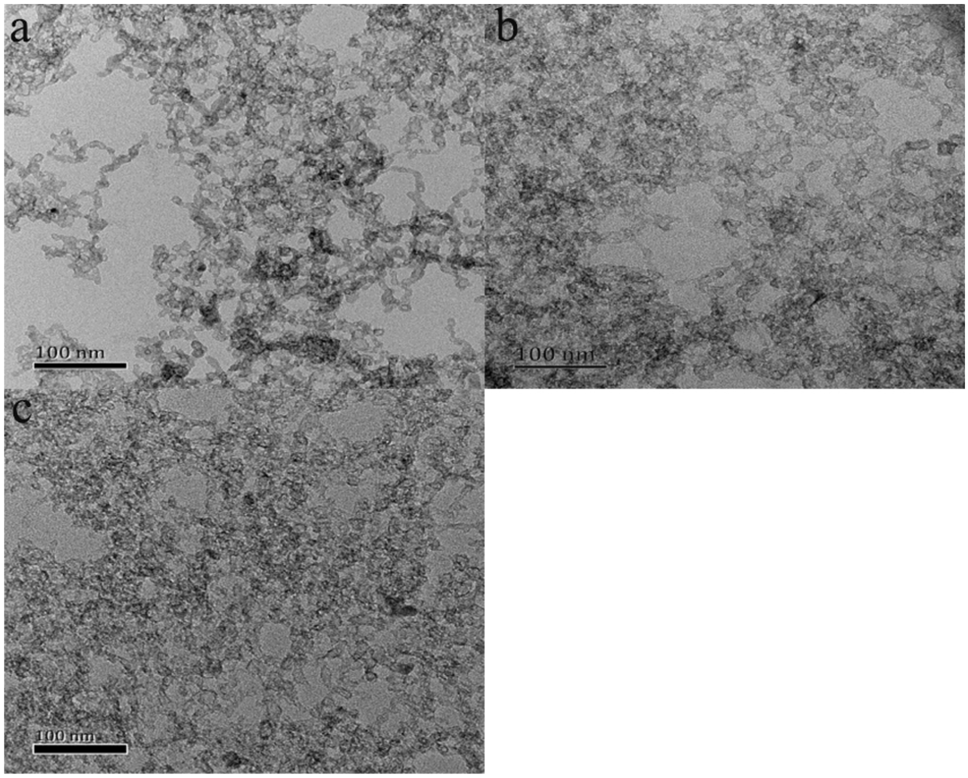

Fig. 6. The TEM images of (a) M-100, (b) M-150, (c) M-200.

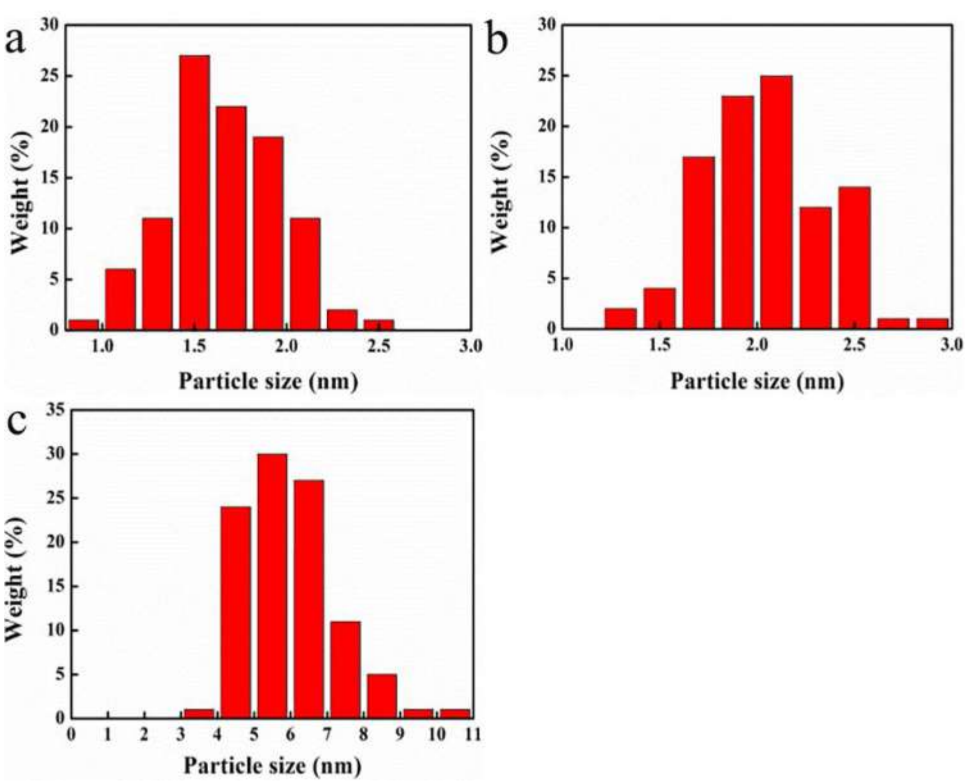

Fig. 7. Particle size distributions of (a) M-100, (b) M-150, (c) M-200.

X", in which X means the reaction temperature. That is, the sols prepared in various reaction temperatures (from 100 to 200 °C) are abbreviated as M-100, M-130, M-160, M-190 and M-210, respectively.

2.5. Preparation of MgF_2-SiO_2 sol

The MgF_2-SiO_2 sol was prepared from the mixture of acid-catalyzed SiO_2 sol and MgF_2 sol having reaction temperature of 200 °C with different SiO_2/MgF_2 sol volume ratio to obtain the suitable refractive

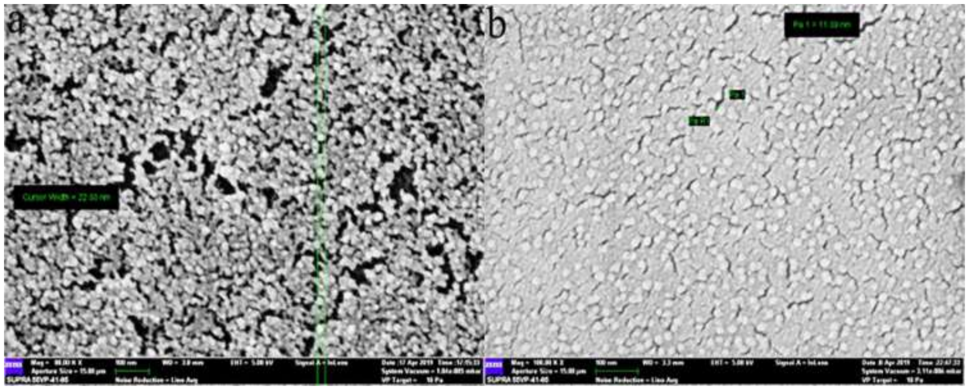

Fig. 8. The FESEM image of SiO_2 coating by different catalysts (a) base ($NH_3 \cdot H_2O$), (b) acid (HNO_3).

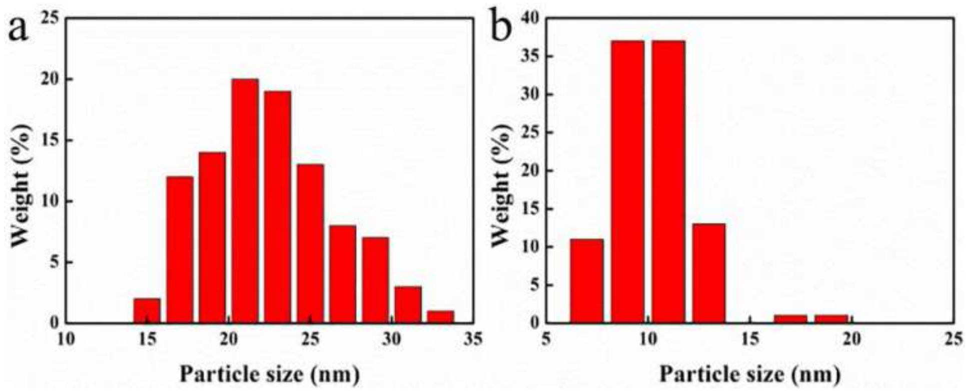

Fig. 9. Particle size distributions of SiO_2 sols prepared by different catalysts (a) base ($NH_3 \cdot H_2O$), (b) acid (HNO_3).

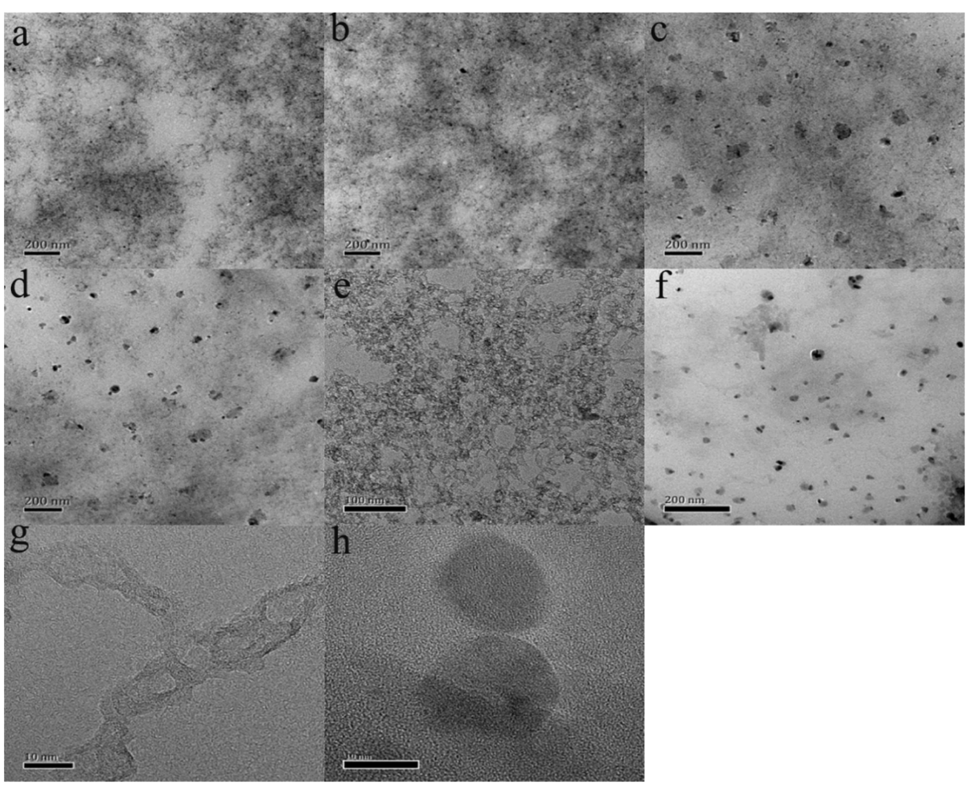

Fig. 10. The TEM images of (a) T-0.1, (b) T-0.2, (c) T-0.3, (d) T-0.4, (e) T-0, (f) pure SiO_2, (g) MgF_2 sol particle, (h) SiO_2 sol particle.

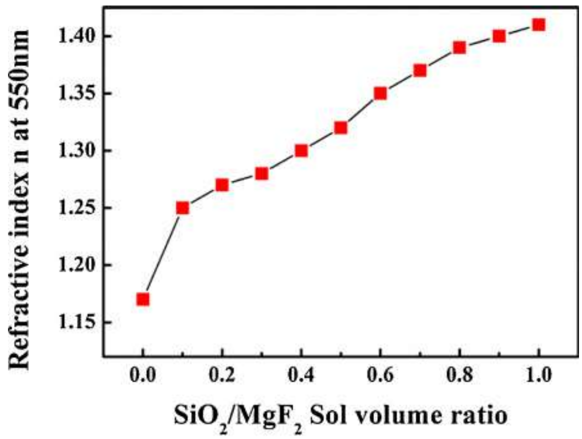

Fig. 11. The refractive index of coatings with different SiO_2/MgF_2 sol volume ratios.

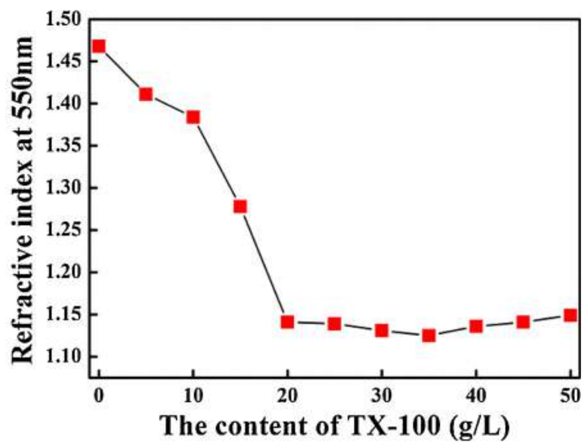

Fig. 12. The refractive index of coatings with different the concentration of TX-100.

Table 3
Different sols used in the various layers that make up the wide-angle broadband ARC.

Layer	1	2	3	4	5
Material (sol)	A-30	A-18	T-0.13	T-0.15	T-0.32

Table 4
Thickness of different types of coatings was measured at different withdrawal rates.

Withdrawal rate (um/s)	300	350	400	450	500	550	600
Layer 1 thickness (nm)	72.3	77.1	79.2	80.9	85.1	87.9	90.2
Layer 2 thickness (nm)	70.1	75.2	77.3	80.1	85.3	86.2	88.7
Layer 3 thickness (nm)	67.1	69.2	71.4	75.1	79.1	81.2	85.1
Layer 4 thickness (nm)	65.1	67.2	70.7	73.8	77.3	81.1	82.1
Layer 5 thickness (nm)	61.2	63.2	65.9	70.1	75.4	78.2	80.5

index. The SiO_2/MgF_2 sol volume ratio was varied from 0 to 1. The sol was noted as MgF_2-SiO_2 sol. The mixed sols are denoted as "T-X", in which X means the SiO_2/MgF_2 sol volume ratio. That is, the sols prepared in various volume ratios (from 0 to 1) are abbreviated as T-0, T-0.1, T-0.13, T-0.15, T-0.18, T-0.2, T-0.3, T-0.32, T-0.35, T-0.38, T-0.4, T-0.5, T-0.6, T-0.7, T-0.8, T-0.9 and T-1, respectively.

2.6. Film deposition

The soda-lime glasses (size: $20 \times 70 \times 1.5mm$ and refractive index n = 1.513) were used as the substrate. It was cleaned and dried through N_2 before deposition. Synthesis of MgF_2-SiO_2 mixed sol for. The bottom layer 3, layer 4 and layer 5 were fabricated using SiO_2/MgF_2 mixed sols with different volume ratios by dip-coating process. The top layer 1 and layer 2 were obtained using SiO_2 sols containing different TX-100 concentrations. The top layers were prepared using SiO_2 sol by sol-gel dip-coating process and coating thickness can be controlled by adjusting the withdraw rate. When each layer of the broadband wide-angle antireflection coating is deposited, the layer 1, layer 2, layer 3, layer 4 and layer 5 will anneal at 300, 300, 200, 200 and 200 °C for 1 h, respectively.

2.7. Characterization

The optical software (Macleod) was used to design wide-angle broadband ARCs and obtain the parameters of each layer of the five-layer coating. The micro-morphology of the coating was observed using a field emission scanning electron microscope (FE-SEM, JSM-IT200, JEOL), and the elemental composition of the coating was analyzed by EDX mapping. The chemical composition of the coating was measured through Fourier transform infrared spectrometer. (FT-IR, IS10, Thermo Scientific). The crystal structure of the coating was observed by X-ray diffraction (XRD, d/max-2400, Rigaku). The transmittance spectrum of substrate coated with wide-angle broadband ARCs was recorded by UV spectrophotometer (UV–vis, UV-3150, Shimadzu). The refractive index and coating thickness were measured by a spectroscopic ellipsometry (Sentech SE800PV). The physical thickness and refractive index of the coating are obtained by an ellipsometer (SE−VM, Yiguang Technology). The structure and morphology of sol particles was shown by transmission electron microscopy (TEM, Zeiss, Libra 120).

The soda-lime glass coated with ARCs was placed on the test bench and fixed, and then the friction device on the test bench was started to wipe the surface of the sample. When the friction times reach to 0, 20, 40, 60 and 70 the average transmittance of the ARCs were measured by the UV–vis spectrophotometer in the range of 400 − 1200 nm. And abrasion resistance of the coating can be measured by studying the change in average transmittance.

3. Results and discussion

3.1. FT-IR, XRD and EDX analysis

Fig. 1 shows the FT-IR spectrum, EDX and XRD images of SiO_2 and MgF_2 coating (Fig. 1 a–f correspond to the base-catalyzed SiO_2 FT-IR, base-catalyzed SiO_2 XRD, MgF_2 EDX, MgF_2 XRD, acid-catalyzed SiO_2 FT-IR and acid-catalyzed SiO_2 FT-IR). The FT-IR spectrum of base-catalyzed SiO_2 coating was demonstrated in Fig. 1(a). It can be seen that the three strong absorption peaks at 1081, 801 and 456 cm^{-1}, corresponding to the antisymmetric stretching vibration of Si-O-Si bond and symmetrical telescopic vibration of Si-O bond [46]. The peaks at 3452 and 1639 cm^{-1}, corresponding to − OH and H − O−H bending vibrations of H_2O. The adsorption of water vapor in the air on the coating surface leads to the appearance of the above two strong absorption peaks [47]. The FT-IR spectrum of acid-catalyzed SiO_2 film was also recorded in Fig. 1(e) and the absorption peaks are basically consistent with the FT-IR of the base-catalyzed SiO_2. The result indicated that the hydrolysis and condensation of TEOS occur in base-catalyzed and acid-catalyzed solution, and a SiO_2 coating was formed on the surface of substrate after annealing.

Moreover, the XRD image of base-catalyzed and acid-catalyzed SiO_2 was shown in Fig. 1(b) and 1(f), respectively. The EDX image of MgF_2 coating was illustrated in Fig.1(c). It can be observed that the fluorine and magnesium elements are present in the coating in an approximate

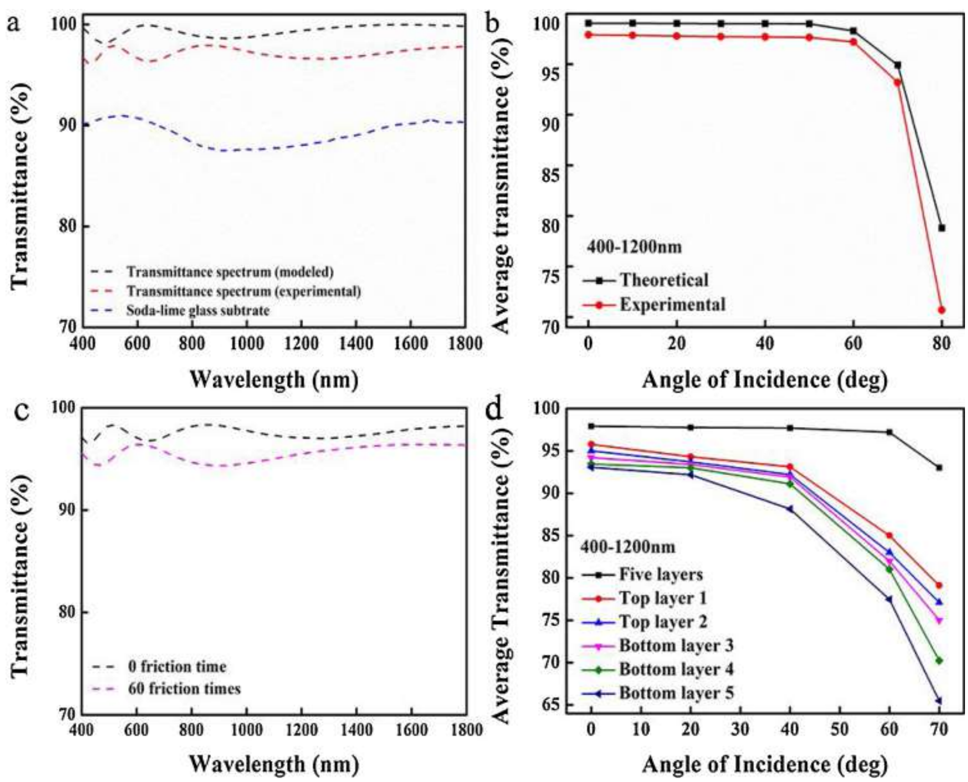

Fig. 13. (a) The transmission spectra of soda-lime glass substrate and coated substrate at the incident angles of 0°. (b) Experimental and modeled average transmittance curves of wide broadband ARCs at an incidence angle of 0-80°. (c) The transmittance spectrum of the ARC before and after rubbing. (d) The average transmittance curves of five layers, top layer1, top layer 2, bottom layer 3, bottom layer 4 and bottom layer 5 ARCs at an incidence angle of 0-70°.

Table 5
Pencil hardness grades for different coatings.

Coating	single layer 1	single layer 2	single layer 3	single layer 4	single layer 5	Five layers
Pencil hardness grade	2B	2B	H	H	2H	2H

ratio of 2: 1. So, this result was confirmed the formation of MgF_2 coating by the EDX mapping. In order to confirm that the coating contains MgF_2-SiO_2 composite material, EDX mapping images were obtained. As shown in Fig.2 a–d, the four chemical elements Si, Mg, O, and F are evenly distributed in the coating. To investigate the effect of doped MgF_2 on the phase structure of SiO_2 samples, XRD analysis was carried out in the range of 10–70° for MgF_2-SiO_2 annealed at 200 °C as shown in Fig. 2(e). Beside, the XRD images of base-catalyzed SiO_2, acid-catalyzed SiO_2, MgF_2 and MgF_2-SiO_2 not show any sharp diffraction peaks. Therefore, these results indicated that base-catalyzed SiO_2, acid-catalyzed SiO_2, MgF_2 and MgF_2-SiO_2 coatings have the property of amorphous structure.

3.2. Optical structure simulation of antireflection film

Wide-Angle broadband ARCs can be designed using many methods. But, these processes are not computer-aided, making the design process complex and time-consuming [48,49]. Computer-aided design is the current mainstream method, due to its clipping, simple and accurate. Therefore, the wide-angle broadband ARCs was be designed by using Macleod.

In order to obtain the optimized parameters, the optical performance of the film was simulated by Macleod. The parameters of each layer of the ARC with the best performance can be seen in Table 1. As shown in Fig. 3, the wide-angle ARCs has better optical property compared to each single layer antireflection coating. Furthermore, the five-layer antireflection coating consist with multilayer graded-refractive-index coatings has excellent broadband antireflection performance in the range of 400 − 1800 nm. Meanwhile, the transmittance of different coatings was simulated at incident angle of 0° to 90° in Fig. 4. It can be obvious that five-layer ARC has wide-angle antireflection property. To further confirm its performance, the transmittance spectrums of different coatings were obtained at incident angle of 70° in Fig. 5. Film consisting of five layers of gradient-index coatings exhibits excellent wide-angle and broadband antireflection capability.

3.3. Effect of reaction temperature on MgF_2 coating

To investigated the effect of reaction temperature on the properties of MgF_2 coatings, the transmittance of the coatings prepared by different groups of reaction temperature and parameters of MgF_2 coating were measured.

Table 2 lists the physico-chemical properties of several MgF_2 coatings prepared via sol-gel process. It can be found that from 100 to 210 °C, the refractive index gradually decrease from approximately 1.35 to 1.15. The relationship between porosity and refractive index was be given by Yoldas and Partlow and this is shown following equation,

$$Porosity = 1 - (n_p^2 - 1)/(n_d^2 - 1) \qquad ((3))$$

Table 6
The average transmittance (400–1200 nm) of the coatings after different friction times.

Friction times	0	5	10	15	20	25	30	35	40
The average transmittance (400 − 1200 nm)	97.9 %	97.8 %	97.6 %	97.3 %	97.1 %	97.0 %	96.9 %	96.7 %	96.5 %

where n^p and n^d represent the refractive index of nanoporous and dense coating, respectively [50]. In this article, n^d is equal to 1.38. According to the Eq. (3), the increase in the porosity of the sample results in a decrease in the refractive index in Table 2. Meanwhile, combined the porosity change increase trend with Eq. (3), our speculation was further confirmed.

To investigate the influence of different temperatures on MgF_2 sol, the microstructure diagram of MgF_2 sol was obtained. As shown in Fig. 6, it can be observed that all the sol particles assume the shape of a linear chain, and there are some cross-links between the particles. However, as the reaction temperature rises, the particles was further cross-linked together, forming lots of big clusters as shown in Fig. 6(b) and (c). This difference may cause changes in the sol particles.

To further confirm our guess, the particle size distributions of the samples at different reaction temperatures were obtained in Fig. 7. By comparing the sol prepared at different temperatures, it can be found that with the enhancing of reaction temperature, particle size of the samples an increasing tendency. When the reaction temperature rose from 100 °C to 150 °C, the average particle size of the sample showed a rapid increase from 1.65 nm to 2.05 nm. When the reaction temperature reached to 200 °C, the average particle size of the sample increased around 5.91 nm. These may be the reasons for the increase in porosity of the sample in Table 2.

3.4. Effect of different catalysts on silica particle size

It is reported that particle size of the sol has a great influence on the mechanical properties of the ARCs. The smaller the particle size of the solution added with MgF_2 sol, the more beneficial it is to enhance the mechanical strength of the coating. To investigate the effect of different catalysts on particle size, FESEM images and particle size distributions of the samples were obtained. As shown in Fig. 8 (a) and (b), the shape of the particles was similar and exhibited spherical. But, it can be observed from the Fig. 8 that the particle size of sample dip-coated in sol with catalyst HNO_3 showed obvious decrease in Fig. 8(b).

The particle size distribution of the processing was shown in Fig.9 to demonstrate the effect of the different catalysts on the SiO_2 sols and coatings. These particle size reductions are visually shown in Fig. 9(a) and (b). When the catalyst is $NH_3{\cdot}H_2O$, the average particle size of the sol particles is 22.6 nm. However, when the catalyst became HNO_3, the average particle size of the sol particles is 10.3 nm. Besides, the porosity of the samples was different. When the catalyst of the sol is $NH_3{\cdot}H_2O$, more pores will be created in the samples dip-coated in sol. According to spectroscopic ellipsometry measurement, the refractive index values of the films dip-coated in acid-catalyzed sol and base-catalyzed sol are roughly 1.46 and 1.15, respectively. This difference may also cause by the change of catalyst type of the sol. Therefore, considering all factors, acid-catalyzed SiO_2 sol is more suitable for adding to MgF_2 sol.

3.5. Properties of MgF_2-SiO_2 coating

According to the theoretical design in section 3.1 above, the refractive index of the third layer, the fourth layer and the fifth layer at the bottom of the coating are 1.20, 1.25 and 1.28, respectively. In order to obtain a suitable refractive index, we mixed acid-catalyzed SiO_2 sol and MgF_2 sol in different volume ratios to prepare MgF_2-SiO_2 composite coatings with adjustable refractive index ranging from 1.15 to 1.46. Fig. 9 shows the TEM image of the MgF_2-SiO_2 mix sol, in which the round and long chain shaded areas are the SiO_2 and MgF_2 particles, respectively. As the volume ratio of acid-catalyzed SiO_2 sol to MgF_2 sol increases from 0 to 0.75, it can be seen that more SiO_2 particles appear in the TEM image. As shown in Fig. 10(g) and (h), it can be obvious that MgF_2 and SiO_2 exhibited the shape of linear chain and spherical particle structure. Particles with a high degree of crosslinking and a linear chain structure are often formed by a sol-gel process. So, the surface of the film composed of these particles has a certain proportion of nanopores. The proportion of nanopores in the film is often greater than 50 %. The mechanical strength of the film became very low due to its high porosity and the low connectivity between particles, and the film could be readily wiped off by a cloth.

As-prepared SiO_2 nanoparticles were very fine particles also in the film strength, it would also cause an increase in the refractive index. But, the pores between the high-crosslinking particle linear structure groups of the film MgF_2 were filled with fine SiO_2 spherical particles to enhance the strength of the coating.

As shown in Fig. 11, a series of coatings with refractive indices ranging from 1.20 to 1.40 were obtained. The layers 3, 4, and 5 with refractive indices of 1.20, 1.25, and 1.28 can be obtained by adjusting the SiO_2/MgF_2 sol volume ratio to 0.13, 0.15, and 0.32, respectively.

3.6. Properties of low refractive index SiO_2 top layer coating

According to the theoretical design in Table 1, when the refractive index of layer 3, 4 and 5 are 1.20, 1.25 and 1.28, the refractive index of the layer 1, 2 will be optimized around 1.12 and 1.15, respectively. We have previously reported a method for the preparation of low refractive index SiO_2 coating with tunable refractive index varying from 1.12 to 1.28 by adding different TX-100 contents in SiO_2 sol. As shown in Fig. 12, the refractive index of the coating is significantly reduced by adding TX-100. However, as the concentration of TX-100 was further increased, the tendency of the refractive index of the coating to decrease gradually stabilized. The top layer 2 with refractive index of 1.15 was prepared by adjusting the concentration of TX-100 to 18 g/L. Besides, the top layer 1 with refractive index of 1.12 was obtained by adjusting the concentration of TX-100 to 30 g/L.

3.7. Effect of withdrawal rate on coating thickness in dip-coating process

The withdrawal rate has a significant effect on the thickness of the coating on the surface of soda-lime glass. The coating thickness in Table 1 of the theoretical design was obtained by adjusting the withdrawal rate. The optimized coating thickness can be obtained by

$$h = C1\left(\frac{\eta V0}{\rho}\right)^{\frac{1}{2}} \tag{4}$$

where h, $C1$, η, $V0$ and ρ were coating thickness, coefficient (0.8), solution viscosity, dip-coating rate and solution density, respectively. But, it is well known that the volume of a coating prepared by the sol-gel process shrinks after annealing. Therefore, the thickness of the coating is calculated using Eq. (4) and a significant error occurs. So, the optimal pulling rate was obtained by ellipsometer testing combined with theoretical calculations. The different sol types used for the coating are shown in Table 3.

As shown in Table 4, different process parameters are shown in order to obtain parameters consistent with the theoretical design. When the withdrawal rates were 350, 450, 550, 550 and 600, respectively, coatings close to the theoretical design thickness were obtained. Due to various factors, the tolerances of thickness and refractive index are controlled within 3.2 %.

3.8. Optical property of five-layer wide-Angle broadband ARC

On the basis of the designed parameters, we have prepared a high-performance wide-Angle broadband ARC using porous SiO_2 coating (n_1 = 1.12, n_2 = 1.15) as top layer and MgF_2-SiO_2 composite coating (n_3 = 1.20, n_4 = 1.25 and n_5 = 1.28) as bottom layer. The wavelength range of the solar radiation spectrum is 400 − 5300 nm. For photovoltaic panels, the main efficient wavelengths of the light for the power generation are 400 − 1200 nm [51]. ARCs mainly increase the power generation of photovoltaic panels by increasing the transmittance of light. Therefore, the optical properties of the coating mainly focus on the transmittance. Fig.13(a) shows the experimental and modeled transmittance spectra of the five-layer ARC annealed at 300 °C. The average transmittance reached 97.90 % at a very broad wavelength range of 400 − 1200 nm, 9% higher than that 88.90 % of the soda-lime glass substrate. Meanwhile, it can be observed that soda-lime glass coated with five layers of coating has excellent wide-angle antireflective performance in Fig.13(c). As shown in Fig.13(b), the transmission spectrum obtained from the experiment of the five-layer wide-angle broadband ARC deviated from the model spectrum at an incident angle of 0°.

3.9. The abrasion-resistance of wide-angle broadband ARCs

In outdoor applications, only high transmittance is not sufficient. Many environmental factors can significantly affect the performance of the coating such as high temperature, high humidity, wind and sand, and various object collisions. Especially for ARC prepared by the sol-gel method, there are many nanopores between the constituent particles of the coating. This feature makes the optical properties of the film unstable because the ARC surface is easily damaged.

As shown in Table 5, pencil hardness grades of different coatings were obtained. It can be seen that by adding MgF_2 sol, the pencil hardness level of the coating is increased from 2B to 2H. To further evaluate the abrasion-resistance of the wide-angle broadband ARCs, the transmittance of the coatings prepared by sol-gel process was measured after different friction times. Table 6 shows the average transmittance of ARCs after 0, 5, 10, 15, 20, 25, 30, 35 and 40 friction times, respectively. It can be observed that the average transmittance does not decrease significantly after the coating is sufficiently rubbed.

For pure MgF_2 sol, the porous network structure will be formed in the process of depositing the coating, which can make the coating have high porosity and low refractive index. But, high porosity can also result in reduced abrasion-resistance property of the film. The MgF_2-SiO_2 composite coating was formed due to the addition of acid-catalyzed SiO_2 sol. The MgF_2-SiO_2 composite coating has a lower porosity and a denser structure than the pure MgF_2. The measurement results of average transmittance indicated that the wide-angle broadband ARC in Table 4 has limited abrasion resistance. Although the top layer of the coating has a loose porous structure due to its ultra-low refractive index, the mechanical properties of the top layer coating cannot meet the requirements. However, the hardness level of the bottom layers was increased by using MgF_2-SiO_2 mixed materials. When the coating was rubbed, the top layer was easily erased due to its weak mechanical properties. But, the bottom layer has good mechanical properties, which can make the ARC have abrasion resistance.

The mechanism of acid-catalyzed SiO_2 sol for improving the abrasion resistance of MgF_2 coatings may require further exploration in the future.

4. Conclusions

In this work, we showed that MgF_2-SiO_2 composite structures coating generated by adding acid-catalyzed SiO_2 sol could be employed to fabricate nanoporous coatings with tunable refractive index over the range 1.46 to 1.15. The five-layer wide-angle broadband ARCs were obtained by combining MgF_2-SiO_2 composite coating with porous SiO_2 coating. Various factors affecting the performance of coatings have been fully investigated, including reaction temperature, type of catalyst, SiO_2/MgF_2 sol volume ratio, TX-100 concentration, withdrawal rate, etc. According to the optimal design parameters optimized by Macleod, the average transmittance of the coating prepared by the sol-gel process reached 97.9 % in the range of 400 − 1200 nm. It can be seen that the coating has outstanding wide-angle antireflection performance through different Transmission spectrum at the angle of incidence. Besides, the wide-angle broadband ARCs have stable optical properties by using an acid-catalyzed SiO_2 sol to improve the process. Therefore, the five-layer wide-angle broadband ARCs can be used in many fields, such as new energy, military equipment and electronic product etc.

CRediT authorship contribution statement

Xiaoyu Sun: Conceptualization, Methodology, Software, Investigation, Writing - original draft. **Jielei Tu:** Resources, Writing - review & editing, Supervision, Data curation. **Lei Li:** Writing - review & editing. **Weinan Zhang:** Resources, Writing - review & editing, Supervision, Data curation. **Kai Hu:** Writing - review & editing.

Declaration of Competing Interest

The authors declare that they have no known competing financial interests or personal relationships that could have appeared to influence the work reported in this paper.

Acknowledgments

This work was supported by National Nature Science Foundation of China (Grant Number 61664010).

References

[1] W. Barthlott, C. Neinhuis, Purity of the sacred lotus, or escape from contamination in biological surfaces, Planta 202 (1997) 1–8.
[2] Y. Du, L.E. Luna, W.S. Tan, M.F. Rubner, R.E. Cohen, Hollow silica nanoparticles in UV–visible antireflection coatings for poly(methyl methacrylate) substrates, ACS Nano 4 (2010) 4308–4316.
[3] D. Chen, Anti-reflection (AR) coatings made by sol–gel processes: a review, Sol. Energy Mater. Sol. Cells (2001).
[4] S. Kitamura, Y. Kanno, M. Watanabe, M. Takahashi, K. Kuroda, H. Miyata, Films with tunable graded refractive index consisting of spontaneously formed Mesoporous silica nanopinnacles, ACS Photonics 1 (2014) 47–52.
[5] J. Yun, T.S. Bae, J.D. Kwon, S. Lee, G.H. Lee, Antireflective silica nanoparticle array directly deposited on flexible polymer substrates by chemical vapor deposition, Nanoscale 4 (2012) 7221–7230.
[6] E. Klobukowski, W. Tenhaeff, J. Mccamy, C. Harris, C. Narula, Atmospheric pressure chemical vapor deposition of high silica SiO_2-TiO_2 antireflective thin films for glass based solar panels, J. Mater. Chem. C 1 (2013) 6188–6190.
[7] K. Pfeiffer, L. Ghazaryan, U. Schulz, A. Szeghalmi, Wide-angle broadband antireflection coatings prepared by atomic layer deposition, ACS Appl. Mater. Interfaces 11 (2019) 21887–21894.
[8] K. Ariga, Y. Yamauchi, G. Rydzek, Q. Ji, Y. Yonamine, K.C.W. Wu, J.P. Hill, ChemInform abstract: layer-by-Layer nanoarchitectonics: invention, innovation, and evolution, Cheminform 45 (2014) 36–68.
[9] G. Zhou, J. He, L. Xu, Antifogging antireflective coatings on Fresnel lenses by integrating solid and mesoporous silica nanoparticles, Microporous Mesoporous Mater. 176 (2013) 41–47.
[10] D. Adak, S. Ghosh, P. Chakrabarty, A. Mondal, H. Saha, R. Mukherjee, R. Bhattacharyya, Self-cleaning V-TiO_2:SiO_2 thin-film coatings with enhanced transmission for solar glass cover and related applications, Sol. Energy 155 (2017) 410–418.
[11] C. Tao, X. Zou, K. Du, G. Zhou, H. Yan, X. Yuan, L. Zhang, Fabrication of robust, selfcleaning, broadband TiO_2-SiO_2 double-layer antireflective coatings with closed-pore structure through a surface sol-gel process, J. Alloys. Compd. 747 (2018) 43–49.
[12] L. Gao, J. He, Surface hydrophobic co-modification of hollow silica nanoparticles toward large-area transparent superhydrophobic coatings, J. Colloid Interface Sci. 396 (2013) 152–159.
[13] J.C. Pouxviel, J.P. Boilot, J.C. Beloeil, J.Y. Lallemand, NMR study of the sol-gel polymerization, J. Non. Solids 89 (1987) 345–360 https://doi.org/10. 1016/S0022-3093(87)80277-6.
[14] K.C. Chen, T. Tsuchiya, J.D. Mackenzie, Sol-gel processing of silica. I. The role of the starting compounds, J. Non. Solids 81 (1986) 227–237.
[15] K. Scheurell, E. Kemnitz, P. Garcia-Juan, J. Eicher, B. Lintner, J. Hegmann, R. Jahn, T. Hofmann, P. L€obmann, Porous MgF_2 antireflective λ/4 films prepared by sol–gel processing: comparison of synthesis approaches, J. Sol. Gel Sci. Technol. 76 (2015) 82–89.
[16] D. Hu, D. Liu, J. Zhang, L. Wu, W. Li, Preparation and stability study of broadband anti-reflection coatings and application research for CdTe solar cell, Opt. Mater. (Amst) 77 (2018) 132–139.
[17] Q. Mu, Y. Li, H. Wang, Q. Zhang, Self-organized TiO2 nanorod arrays on glass substrate for self-cleaning antireflection coatings, J. Colloid Interface Sci. 365 (2012) 308–313.
[18] G. Dingemans, W.M.M. Kessels, Status and prospects of Al2O3-based surface passivation schemes for silicon solar cells, J. Vac. Sci. Technol. 30 (2012) 040802.
[19] D. Li, F. Huang, S. Ding, Sol–gel preparation and characterization of nanoporous

ZnO/SiO2 coatings with broadband antireflection properties, Appl. Surf. Sci. 257 (2011) 9752–9756.
[20] X. Sun, X. Xu, J. Tu, P. Yan, G. Song, L. Zhang, W. Zhang, Research status of antireflection film based on TiO_2, IOP Conf. Ser. Mater. Sci. Eng 490 (2019).
[21] S. Hao, T. Lin, S. Ning, Y. Qi, Z. Deng, Y. Wang, Research on cracking of SiO2 nanofilms prepared by the sol-gel method, Mater. Sci. Semicond. Process. 91 (2019) 181–187.
[22] K. Ding, X.J. Zhang, L. Ning, Z.B. Shao, P. Xiao, A. Ho-Baillie, X.H. Zhang, J.S. Jie, Hue tunable, high color saturation and high-efficiency graphene/silicon heterojunction solar cells with MgF_2/ZnS double anti-reflection layer, Nano Energy 46 (2018) 257–265.
[23] K. Choi, K.J. Kim, Antireflection coating of a SiO/SiN double layer on silicon fabricated by magnetron sputtering, J. Ceram. Process. Res. 3 (2010) 341–343.
[24] T. Sertel, N.A. Sonmez, S.S. Cetin, S. Ozcelik, Influences of annealing temperature on amorphous Ta_2O_5 thin films anti-reflective performance of, Ceram, Int. 45 (2018) 11–18.
[25] K.X. Dong, D.J. Chen, H.F. You, Y.J. Wang, Y.Y. Zhang, X.X. Wang, Growth and characteristics of SiO_2/Si_3N_4 photonic crystal filter with anti-reflection coatings, Nnanosci. Nanotech. Let. 11 (2019) 257–265.
[26] D. Li, F. Huang, S. Ding, Sol–gel preparation and characterization of nanoporous ZnO/SiO_2 coatings with broadband antireflection properties, Appl. Surf. Sci. 257 (2011) 9752–9756.
[27] R. Prado, G. Beobide, A. Marcaide, J. Goikoetxea, A. Aranzabe, Development of multifunctional sol–gel coatings: anti-reflection coatings with enhanced self-cleaning capacity, Sol. Energy Mater. Sol. Cells 94 (2010) 1081–1088.
[28] C.C. Katsidis, D.I. Siapkas, General transfer-matrix method for optical multilayer systems with coherent, partially coherent, and incoherent interference, Appl. Opt. 41 (2002) 3978–3987.
[29] C. Agustín-Sáenz, M. Machado, O. Zubillaga, A. Tercjak, Hydrophobic and spectrally broadband antireflective methyl-silylated silica coatings with high performance stability for concentrated solar applications, Sol. Energy Mater. Sol. Cells 200 (2019).
[30] J.Y. Chen, K.W. Sun, Growth of vertically aligned ZnO nanorod arrays as antireflection layer on silicon solar cells, Sol. Energy Mater. Sol. Cells 94 (2010) 930–934.
[31] G. San Vicente, R. Bayón, N. Germán, A. Morales, Surface modification of porous antireflective coatings for solar glass covers, Sol. Energy 85 (2011) 676–680.
[32] G. San Vicente, R. Bayón, N. Germán, A. Morales, Long-term durability of sol-gel porous coatings for solar glass covers, Thin Solid Films 517 (2009) 3157–3160.
[33] M.R. Maghami, H. Hizam, C. Gomes, M.A. Radzi, M.I. Rezadad, S. Hajighorbani, Power loss due to soiling on solar panel: a review, Renewable Sustainable Energy Rev. 59 (2016) 1307–1316.
[34] Rao, R. Pillai, M. Mani, P. Ramamurthy, Influence of dust deposition on photovoltaic panel performance, Energy Procedia 54 (2014) 690–700.
[35] S. Mekhilef, R. Saidur, M. Kamalisarvestani, Effect of dust, humidity and air velocity on efficiency of photovoltaic cells, Renewable Sustainable Energy Rev. 16 (2012) 2920–2925.
[36] F. Mejia, J. Kleissl, J.L. Bosch, The effect of dust on solar photovoltaic systems, Energy Procedia 49 (2014) 2370–2376.
[37] V. Sharma, S.S. Chandel, Performance and degradation analysis for long term reliability of solar photovoltaic systems: a review, Renewable Sustainable Energy Rev. 27 (2013) 753–767.
[38] S.A. Sulaiman, A.K. Singh, M.M.M. Mokhtar, M.A. Bou-Rabee, Influence of dirt accumulation on performance of PV panels, Energy Procedia 50 (2014) 50–56.
[39] G.I. Cooper, Ga. Cox, The aqueous corrosion of potash-lime-silica glass in the range 10–250 °C, Appl. Geochem. 11 (4) (1996) 511–521.
[40] M. Vilarigues, R.C. da Silva, Characterization of potash-glass corrosion in aqueous solution by ion beam and IR spectroscopy, J. Non-Cryst. Solids 352 (50–51) (2006) 5368–5375.
[41] C. Tao, L. Zhang, Fabrication of multifunctional closed-surface SiO2-TiO2 antireflective thin films, Colloids Surf. A Physicochem. Eng. Asp. 585 (2019).
[42] Jannat, W. Lee, M.S. Akhtar, Z.Y. Li, O.B. Yang, Low cost sol–gel derived SiC–SiO_2 nanocomposite as antireflection layer for enhanced performance of crystalline silicon solar cells, Appl. Surf. Sci. 369 (2016) 545–551.
[43] S. Lien, D. Wuu, W. Yeh, J. Liu, Tri-layer antireflection coatings (SiO_2/SiO_2–TiO_2/TiO_2) for silicon solar cells using a sol–gel technique, Sol. Energy Mater. Sol. Cells 90 (2006) 2710–2719.
[44] S. Hao, T. Lin, S. Ning, Y. Qi, Z. Deng, Y. Wang, Research on cracking of SiO_2 nanofilms prepared by the sol-gel method, Mater. Sci. Semicond. Process. 91 (2019) 181–187.
[45] A.F. Werner Stöber, Controlled growth of monodisperse silica spheres in the micron size range, J. Colloid Interface Sci. 26 (1968) 62–69.
[46] X. Huang, Y. Yuan, S. Liu, W. Wang, R. Hong, One-step sol-gel preparation of hydrophobic antireflective SiO2 coating on poly(methyl methacrylate) substrate, Mater. Lett. 208 (2017) 62–64.
[47] H.S. Chen, Z.Y. Sun, J.C. Shao, Investigation on FT-IR spectroscopy for eight different sources of SiO2, Bulletin of the Chinese Ceramic Society 30 (2011) 934–937.
[48] L. Yan, F. qin Dong, S. Zhao, H. Yan, H. Lv, X. Yuan, Hydrophobic MgF2 antireflective films with enhanced environmental durability by a sol–gel process, Mater. Lett. 129 (2014) 156–158.
[49] X.X. Zhang, S. Cai, D. You, L.H. Yan, H.B. Lv, X.D. Yuan, B. Jiang, Template-free sol-gel preparation of superhydrophobic ORMOSIL films for double-wavelength broadband Antirefl ective coatings, Adv. Funct. Mater. 23 (2012) 4361–4365.
[50] B.E. Yoldas, D.P. Partlow, Formation of broad band antireflective coatings on fused silica for high power laser applications, Thin Solid Films 129 (1985) 1–14.
[51] A. Pan, H. Lu, L.-Z. Zhang, Experimental investigation of dust deposition reduction on solar cell covering glass by different self-cleaning coatings, Energy 181 (2019) 645–653.